Journal of Power Sources 373 (2018) 40–53

Contents lists available at ScienceDirect

Journal of Power Sources

journal homepage: www.elsevier.com/locate/jpowsour

A quick on-line state of health estimation method for Li-ion battery with incremental capacity curves processed by Gaussian filter

Yi Li[a,b,*], Mohamed Abdel-Monem[a,c], Rahul Gopalakrishnan[a], Maitane Berecibar[a], Elise Nanini-Maury[b], Noshin Omar[a], Peter van den Bossche[a], Joeri Van Mierlo[a]

[a] Vrije Universiteit Brussel, MOBI Research Group, Pleinlaan 2, 1050, Brussels, Belgium
[b] ENGIE LAB Laborelec, Rodestraat 125, B-1630, Linkebeek, Belgium
[c] Helwan University, Faculty of Engineering, Cairo, Egypt

HIGHLIGHTS

- Proposed an on-line battery state of health (SoH) monitoring method for NMC cells.
- The method can monitor battery SoH with partial charging data.
- Ageing mechanisms of batteries are studied by non-destructive methods.
- Gaussian filter is used to obtain IC curves with improved smoothness.
- Established a quantitative correlation between features on IC curves and cell SoH.

ARTICLE INFO

Keywords:
On-line SoH estimation
High energy NMC batteries
Ageing mechanism
Incremental capacity
Differential voltage
Gaussian smoothing

ABSTRACT

This paper proposes an advanced state of health (SoH) estimation method for high energy NMC lithium-ion batteries based on the incremental capacity (IC) analysis. IC curves are used due to their ability of detect and quantify battery degradation mechanism. A simple and robust smoothing method is proposed based on Gaussian filter to reduce the noise on IC curves, the signatures associated with battery ageing can therefore be accurately identified. A linear regression relationship is found between the battery capacity with the positions of features of interest (FOIs) on IC curves. Results show that the developed SoH estimation function from one single battery cell is able to evaluate the SoH of other batteries cycled under different cycling depth with less than 2.5% maximum errors, which proves the robustness of the proposed method on SoH estimation. With this technique, partial charging voltage curves can be used for SoH estimation and the testing time can be therefore largely reduced. This method shows great potential to be applied in reality, as it only requires static charging curves and can be easily implemented in battery management system (BMS).

1. Introduction

Lithium ion battery (LIB) was firstly commercialized by Sony in 1991, since then this chemistry has become the one of the most promising and fastest growing electric energy system storage (ESS) in the market due to the advantage of high volumetric/gravimetric energy density [1]. LIBs were initially applied on portable/consumer devices such as cell phones and laptops, with the achieved significant success in this market, they are recently penetrating into the field of hybrid electric vehicle (HEVs) and electric vehicles (EVs). It could be foreseen that they can largely expand their market in large scale ESS application as their costs keep dropping and the lifetime get improved [2].

The performance of LIB degrades with time, an accurate diagnosis of battery degradation is of great significance for safe and efficient battery utilization. Battery state of health (SoH) is used as an indicator to evaluate the degradation level of batteries. The battery SoH is monitored through a battery management system (BMS), it still remains a difficult and challenging topic since the ageing mechanisms of batteries are complicated and the battery degradation do not originate from one single cause, but from various processes and their interactions, like the operating modes, working environment and ageing history [3,4]. The battery SoH reflects the ability of a battery to store and supply energy in respect to its initial conditions by considering the energy and power requirements of the application, which can be defined as a state of

* Corresponding author. Vrije Universiteit Brussel, MOBI Research Group, Pleinlaan 2, 1050, Brussels, Belgium.
E-mail address: li.yi@vub.be (Y. Li).

http://dx.doi.org/10.1016/j.jpowsour.2017.10.092
Received 27 June 2017; Received in revised form 30 October 2017; Accepted 31 October 2017

health related to energy capability (SoH_E) or/and power capability (SoH_P). The SoH_E can be quantified by the battery capacity and impedance is used for the quantitative definition of battery SoH_P. Having an accurate prediction for either one with simple approaches is particularly significant to the safety of entire systems, with this information we can adjust the operating modes to extend the battery lifetime as well as predict the appropriate time intervals for battery replacement [5]. In this work, the battery capacity is chosen as the indicator for SoH by calculating the ratio of actual cell capacity to the cell initial capacity ($SoH = \frac{Q_{current}(Ah)}{Q_{fresh}(Ah)} \times 100\%$). For a fresh battery, the SoH is equal to 100% and the value of SoH decreases with ageing. The battery end of life (EoL) is defined by the application requirements. For the batteries applied in EVs or HEVs, they are considered no longer usable and should be replaced when the SoH is less than 80% [6]. However, this direct calculation method requires a fully charging and discharging cycle of the battery, which is energetically inefficient as well as impractical in real application since the batteries are partially cycled in most cases.

Research on battery SoH estimation has attracted lots of attention in recent years. Different estimation methods have been proposed in this field, each technique has its own advantages and shortcomings in terms of estimation accuracy, testing time duration, feasibility for implementation. The SoH estimation techniques can be roughly classified to three groups: experimental techniques, adaptive models and incremental capacity/differential voltage analysis.

The first group is directly measured from experiments, such as hybrid pulse power characterization (HPPC) and electrochemical impedance spectroscopy (EIS). HPPC method is capable of identifying the battery dynamic power capability over its useable charge and voltage range by using a test profile that incorporates both charge and discharge pulses [5,7]. EIS is mainly used to determine the impedances of the battery and proved to be an effective tool for ageing and failure diagnosis [8,9]. Since the battery impedance increases with battery capacity fade and different battery dynamics tend to affect different frequency ranges on the EIS measurement [5]. However, the experimental methods are remaining to be off-line SoH identification techniques [9].

The second group is the adaptive model based methods, which can be further dived into lumped-parameter equivalent circuit based models and black-box based methods. The equivalent circuit model (ECM) with joint/dual extended Kalman Filters (EKF), also called joint estimation, have the advantages of providing high accuracy of capacity estimation [10–15]. These models have strong physical relation between the model parameters with the underlying electrochemical processes that occur within battery cells [16]. Unfortunately, the model based techniques can be computational intensive due to large matrix operations and therefore difficult to be implemented in BMS for real application [15]. The black-box based models, such as neuron network (NN) and support vector regression (SVR), do not rely on the predetermined system parameters or have any connection with the physical properties of batteries [10,17–20]. Compared to model-based approaches, they have less requirements on dedicated hardware/software [17]. Such statistical approach learns the ageing behavior of the studied system from a large amount of data and find a mathematical description to make connections between the battery features like terminal voltage, current and temperature with the cell capacity. The limitation of the machine learning based method is that they require acquisition of data covering the entire age of the battery under various utilization modes, and they are only valid within the trained data range [18].

The third group is the differential approach based on incremental capacity (IC) analysis and/or differential voltage (DV) analysis. This differential analysis have the advantages from both experimental and adaptive-model approaches, as it can be used for battery degradation identification as well as the SoH estimation with low computational effort [6]. The requirement of static charging/discharging is the main drawbacks of this method [6]. Incremental capacity is calculated by differentiating the change in battery capacity to the change in terminal voltage during either charging or discharging, as defined in the Eq. (1). Differential voltage is defined as the inverse of differential capacity, shown in Eq. (2) [21].

$$\frac{dQ}{dV} = \frac{\Delta Q}{\Delta V} = \frac{Q_t - Q_{t-1}}{V_t - V_{t-1}} \tag{1}$$

$$\frac{dV}{dQ} = \frac{\Delta V}{\Delta Q} = \frac{V_t - V_{t-1}}{Q_t - Q_{t-1}} \tag{2}$$

where Q_t and represent the battery capacity and voltage at time t, respectively. Although both of them can provide similar information, there is a big difference between each other. The IC curve refers to the cell voltage, which can be a direct indicator of the battery state, whereas the DV refers to the cell capacity, which is a secondary indicator that can vary with aging and degradation and lose its reliability as a reference in the course of aging [22]. With this method, the voltage plateaus on the charging/discharging curve can be transformed into clearly identifiable peaks on the IC/DV curve. The peaks in IC curve represent phase equilibria, while the DV curve represents phase transitions [23]. Each peak in the curve has its unique features, like intensity and position, and it represents a specific electrochemical process taking place in the cell [24]. The extracted peak values and the shape and position variation of peaks are closely related to the battery capacity fading, and therefore can be used for monitoring battery ageing. The specific degradation mechanism can be distinguished by analyzing the progression of each peak in IC/DV curves throughout ageing, observing how the change of the active materials over time can be helpful in identifying the best operating conditions for cells.

Previous studies based on differential analysis have shown it to be an effective tool for both analyzing battery ageing mechanism and SoH estimation, e.g. in Refs. [4,6,25–32]. This method is interesting as it have many advantages: it can be easily implemented in a BMS by just monitoring two parameters (voltage and charge/discharge capacity); it is suitable for different types of lithium ion batteries like chemistries, battery size, cell designs and operating condition [5]. Bloom et al. [30] conducted DV analysis on NMC/graphite cells and found the side reactions mainly happen on negative electrode which leads to battery capacity fade. Han et al. [29] used IC curves to analyze the ageing mechanism of NMC/LTO cells and found a two-stage capacity loss, which is caused by the loss of anode material and loss of cathode material, respectively. Dubarry et al. [28] studied the aging behaviors of commercialized $LiFePO_4$ /graphite (LFP) cells in different formats with IC analysis. Till now, most of the IC/DV analysis on Li-ion batteries have been focused on the electrochemical ageing mechanism analysis, while only a handful of research has been carried out for on-line SoH estimation [4,6,31,32]. Wang et al. [4] proposed an on-line SoH estimation method for LFP battery pack, they estimated the battery SoH by relating the location interval of two inflection points on DV curves to battery capacity fade. Berecibar et al. [6] estimated the battery SoH with DV analysis, their method is able to use partial charging curves with maximum initial SoC levels of 60% SoC but restricted to low charging current rate ofI_t[1]/5. Weng et al. [31] derived IC curves with the approach of support vector regression algorithm by using partial charging data and the battery capacity fade was correlated with the intensity of IC curve peaks, but it is costly to be implemented into BMS. These IC/DV based SoH estimation techniques are developed for LFP cells. Because each chemistry has its own characteristics and performs differently from the others, this means the proposed method for LFP cells might not be suitable for NMC cells. Therefore, the adaptability and validity of IC/DV analysis on NMC cells should be investigated. Goh et al. [32] proposed a capacity estimation algorithm for NMC battery by using second-order DV curves obtained in the constant charging phase,

[1] I_t represents the current rate as documented in the standard IEC 61434 and presented by Equation I_t = C/1 h [33].

nevertheless, this method has the limitation of requiring a low initial charging SoC level (less than 15%). There is still room for the improvement of IC/DV analysis for SoH estimation, like reducing the testing time by increasing current rate and/or using partial charging/discharging curves with flexible initial charging SoC levels.

To get IC/DV curves, applying numerical derivative directly to the data is the most intuitive approach as shown in Eqs. (1) and (2). The peaks of IC curves are derived from the voltage plateau region of the voltage-capacity curve, and this region is sensitive to measurement noise and trembling [31,34]. Getting smoothed IC/DV curves is the first and also the most important step for further ageing and SoH analysis. Till now, different methods have been applied to obtain smooth IC/DV curves, like moving average (MA) [23,25,26,30,35], improved center least squares method [4], applying radial basis function [21], support vector regression [31] and data reduction prior to applying derivative functions (e.g. using the experimental data with 10 mV intervals) [36]. Among all, MA is one of the most often used methods due to its simplicity. MA is good enough for distinguishing the important features on the differential curves, but it fails to provide satisfying smoothing effect for on-line SoH estimation. The detailed discussion of MA will be thoroughly discussed in Section 3.1. In order to obtain IC/DV curves for quantitative analysis, an improved smoothing method with enough simplicity for further being implemented in BMS is highly wanted.

This paper aims at developing a fast on-line SoH monitoring method with differential analysis for high energy NMC/graphite LIBs. Our study is based on a battery life cycle test data set with more than two-year experimental period. In this work, an advanced smoothing method based on Gaussian filtering is proposed, which has proved to be an effective method for obtaining smooth differential curves and preserving well the important features on the curves that show strong correlation with battery ageing. An effective on-line SoH estimation method was proposed based on the IC analysis with $I_t/2$ current rate during charging process, which can largely reduce the time for battery SoH estimation. The results show that the proposed method built up on the data from one cell is able to predict the SoH of five other cells which are cycled under different cycling depth with less than 2.5% max errors. The proposed multi-stage SoH estimation method is valid to identify the battery SoH with only partial charging, and the testing time can be therefore largely decreased from maximum 2 h to minimum 0.8 h under test current rate. Since battery SoH estimation is closely related to the ageing process, work was also carried out on discussing the degradation mechanisms of the high energy NMC batteries with low current test profile of $I_t/25$.

The remainder of this paper is organized as follows: Section 2 introduces experiment setup and cycle ageing framework. In Section 3, the constrains of conventional smoothing method for obtaining IC/DV curves are discussed and an advanced smoothing technique based on Gaussian filtering is proposed. The physical battery degradation process is discussed in Section 4 by analyzing the IC/DV curves obtained from $I_t/25$ test. Section 5 proposed the on-line SoH estimation method by analyzing the variation of features on the IC curves with ageing, the validation of this method is also presented in this section. The conclusions are presented in Section 6.

2. Experimental

2.1. Cell specifications and testing system

The batteries used for this test are commercial high energy NMC/graphite pouch cells. We could not establish the name of the manufacturer. The nominal capacity of the battery is 31.5 Ah, and voltage operation range is from 3 V to 4.2 V. The parameters of the battery cells used in the tests are listed in Table 1. The whole ageing tests were performed in ambient temperature.

The experiments were performed on a 16-channel, SBT05250L type battery test system manufactured by PEC with a current range of 0–250 A and a voltage range of 0–5 V. The voltage and current accuracy are ± 0.03% full scale. The data acquisition system has a sampling frequency of max. 100 Hz.

Table 1
Specifications of tested cells according to the manufacturer's datasheet.

Positive electrode material	NMC
Negative electrode material	Graphite
Nominal capacity (at $0.3I_t$ rate, 3 V–4.2 V)	$31.5Ah \pm 2.5\%$
Nominal voltage (at $0.3I_t$ rate)	3.7 V
Energy density	180 $Wh{\cdot}kg^{-1}$
Power density (at 50% SoC, 10 s)	2300 $W{\cdot}kg^{-1}$
Voltage range	3 to 4.2 V

Table 2
Test matrix for cycling ageing.

Specifications	Cell 1	Cell 2	Cell 3	Cell 4	Cell 5	Cell 6
Cycle depth (%)	100	100	80	80	60	60
Cycling SoC range (%)	0–100	0–100	20–100	20–100	40–100	40–100

2.2. Battery ageing test profiles

The battery ageing process are influenced by many factors like cycling depth, current rate, temperature and middle state of charge. All the factors work simultaneously on the batteries to influence the capacity and power degradation. For a specific application, however, some of the stress factors can play more important roles on the battery ageing than the others. We could investigate the battery degradation process by focusing on the most important ageing impact factors. Due to the application requirement, our research work is mainly interested in the impact of cycling depth on the battery capacity fading process.

A CC-CV (constant current - constant voltage) charge-discharge test regime is used to age the battery. During charging, the current rate of $I_t/2$ is applied on the CC step until the battery reaches its cut-off voltage of 4.2 V. Then a CV step in which battery remain in floating mode at the cut-off voltage until the current reaches the minimum threshold of $I_t/10$. Then the batteries are discharged with the same current rate of $I_t/2$ till the predefined lower voltage limit. Six cells in total are used for cycling ageing test, divided into three groups and cycled under different cycling Depth of Discharge (DoD). The selected cycling DoD levels are 100%, 80% and 60%, the DoD always refers to the nominal capacity as indicated by the battery manufacturer in this work. The cycle test matrix is given in Table 2. Cell 1 and 2 are cycled under 100% DoD, it refers to a complete discharge from 100% SoC to 0% SoC and a complete charge process from 0% to 100% SoC. Similarly, the cell 3 and 4 are cycled under 80% DoD refer to discharge and charge process in the SoC range of 100%–20%, and cell 5 and 6 cycled under 60% DoD are discharged and charged in the range of 100%–40% SoC.

In this test, capacity tests have been performed with intervals of every 100 full equivalent cycles (FECs)[2] to assess the battery capacity loss. The capacity test at beginning of life (BoL) allows us to collect the information of the initial condition of the battery, and it determines the baseline values of battery health, which are later used to enable health monitoring throughout the useful life of the battery. The periodic characterization tests performed during cycling intervals allow us to

[2] One equivalent full cycle means one complete charge and discharge event. However, cells are not always going from fully charged to discharged state, but in partial cycle range (e.g. from 20% to 100% SOC range) or in irregular operating conditions (e.g. real driving cycles). In such cases, the number of equivalent cycles can be calculated: $N = \sum(\Delta DoD/2)$. If a battery is charged from fully discharged (0% SOC) to fully charged (100% SOC), the ΔDOD is 1 for both charging and fully discharging step, producing one equivalent cycle according to the equation.

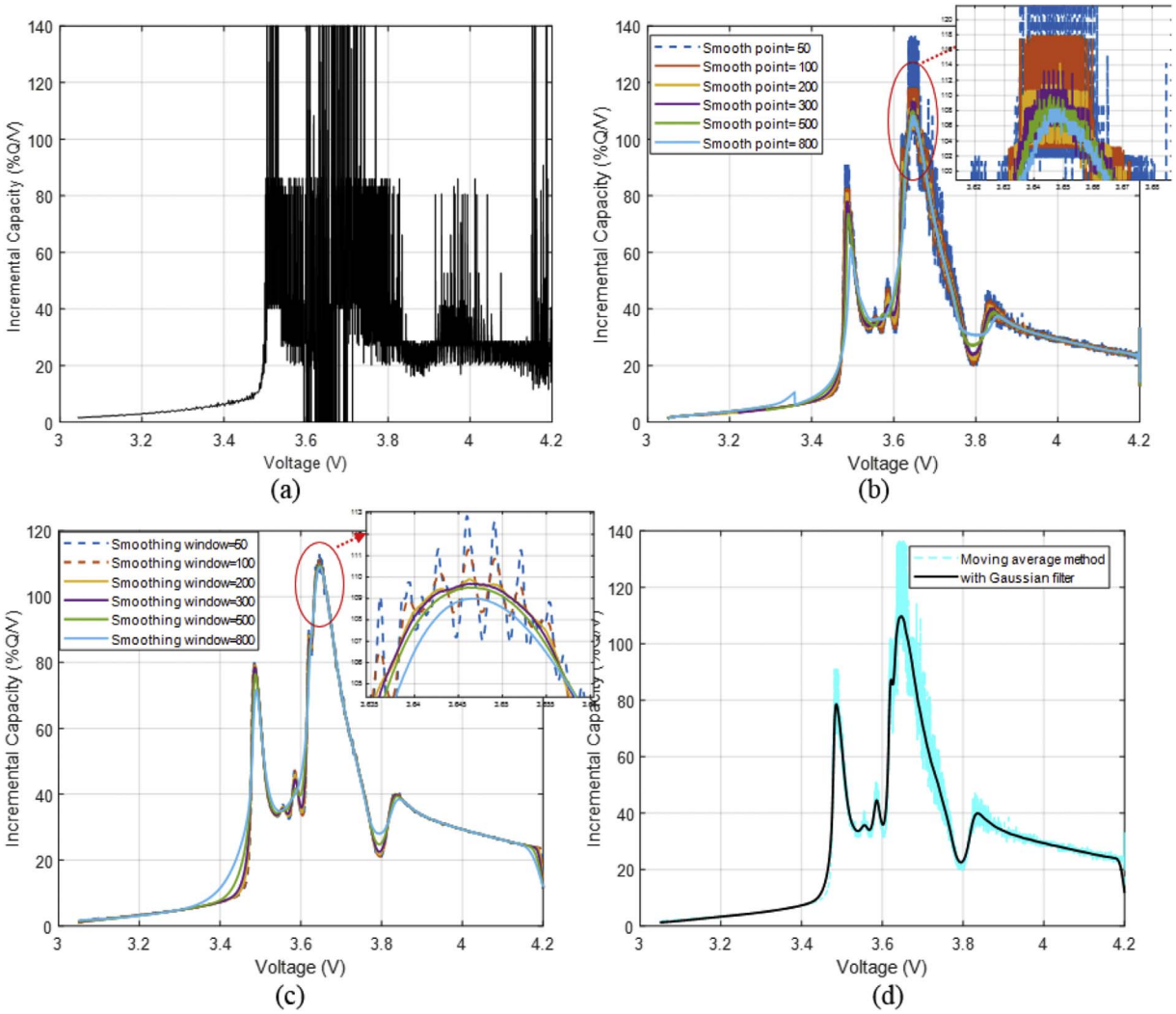

Fig. 1. IC charge curve(s) of cell 1 at BoL under current rate of $I_t/25$ with sampling frequency of 0.1 Hz (a) without applying smoothing tool (b) after applying average smoothing methods with different smooth points of 50, 100, 200, 300, 500 and 800 (c) comparison of IC curves smoothed by GS with smoothing window of 50, 100, 200, 300, 500 and 800 (d) comparison of two smoothing method: MA method with smoothing points of 50 and proposed GS with smoothing window of 300.

acquire information on the battery ageing trends. CC-CV mode is used for performing the capacity test with highest and lowest cut-off voltage of 4.2 V and 3.0 V, respectively. The capacity tests were carried out at different current rates: $I_t/25$, $I_t/3$, $I_t/2$ and $1I_t$. The purpose of the capacity test at low current rate of $I_t/25$ is to identify the battery ageing mechanism with IC/DV analysis. At such low constant current, full charge and discharge tests are able to measure the amount of accessible capacity of the cell and to determine the relationship between the cell potential and capacity under quasi-equilibrium conditions. The resulting charge and discharge curves contain electrode phase information with a minimum amount of kinetic artifacts and are well suited for degradation mechanism analysis. However, carrying out capacity test at such low current rate is not practical for real application of SoH estimation due to being time consuming. Therefore, the capacity test at higher current rate was carried out to find the most suitable current rate for on-line SoH identification in a reasonable time period without compromising the estimation accuracy.

3. IC/DV curve acquisition

The battery discharge process is unpredictable as this process depends on the utilization mode of the battery system. Nevertheless, the charge current is normally constant under most conditions like charging of electrical vehicles. Therefore, the charging voltage-capacity(V-Q) curve is chosen for IC/DV analysis for battery SoH estimation.

3.1. Conventional numerical derivative with moving average (MA) smoothing

Fig. 1 (a) gives an example of the IC curve for cell 1 at fresh state achieved by numerical derivative method, the measurements were collected with 10 s intervals (Sampling frequency = 0.1 Hz, the reason of using this time interval will be discussed in Section 3.3). All single cell results in this paper are based on the cell 1 unless otherwise notified. As observed, this curve is very noisy and it is impossible to identify any useful features. In order to get a smoother differential curves, MA is normally applied on the battery voltage and capacity data before applying the numerical-derivative method. MA is a specified number of past data points, giving equal weight to each data point. The moving average filter can be expressed as [37]:

$$y(i) = \frac{1}{M}\sum_{j=0}^{M-1} x(i+j) \tag{3}$$

where x(·) is the input signal, y(·) is the output signal, and M is the number of points in the average. With this moving average filter, the random white noise can be reduced while the sharpest step response is sustained [38]. MA is highly influenced by the number of chosen

smoothing points. Increasing the number of smoothing points can give improved smoothing effect but the shape of obtained curves will be deformed and can therefore lead to false interpretation of the important features on the IC/DV curves.

Fig. 1 (b) illustrates the influence of different smoothing points on the IC curves for a fresh cell. Although the peaks can be clearly seen from the IC curve with smoothing points of 50, it is still too noisy to be used for further investigation since the important information like peak height or position cannot be identified from it. To achieve a smoother curve, the smoothing points need to be increased. Nevertheless, the increment of the smooth points leads to the deformation of curves. The intensity of all peaks are decreasing and the positions of them are shifting toward to higher voltage range along with the increased smoothing points. Additionally, the small peaks in the voltage range of 3.5–3.6 V are diminished when the smoothing points increase to 800. Unfortunately, with largely increased smoothing points, the smoothing effect of MA method is still not satisfying for accurately extracting the information of peak features like position and intensity. This can be seen from the small figure in Fig. 1 (b). Therefore, MA method is not suitable for further quantitative analysis and a more robust method is required to provide improved curve smoothing effect as well as conserve all the important features on IC curves.

3.2. Improved smoothing method with Gaussian smoothing (GS)

Herein, Gaussian filter is introduced on the sets of pre-filtered data with MA to give satisfactory reductions of the variability. The key to the success of this technique lies in the fact that the data were dominated by relatively low frequencies of variation which could be separated from the higher frequency noise.

The GS is highly accurate where they confidently identify signatures. A GS has the shape of a Gaussian distribution, which is expressed with the following equation [39]:

$$G(x) = \frac{1}{\sigma\sqrt{2\pi}} exp\left(\frac{-(x-\mu)^2}{2\sigma^2}\right) \quad (4)$$

where μ is the mean value, and σ is standard deviation controls the window size. The moving averaging filter mentioned above can replace each data point with the average of its neighbors. This means that nearby data all play an equal role in the average and the distant data play no role. When Gaussian filter is applied, each data point can be replaced by a weighted average of its neighbors. Hence, the nearest data have more influence on the average and the distant data play a smaller role. When the Gaussian is used for smoothing, μ is normally set to 0, because we want each data to be the one that has the biggest effect on its new, smoothed value. σ will serve as a parameter that allow us to control how much smooth the final curve, more specifically, how big the smoothing window we use for averaging. The bigger σ is, the smoother effect we can achieve. Nevertheless, the value of σ should be kept in an appropriate range. Too small a value leads to undesirable smoothing effect, while too large a value may result in losing important information.

After generating a Gaussian window with the aforementioned equation (using *gausswin*(N), a function in the statistics toolbox for Matlab, N defines the Gaussian window point number), it will be convolved with the pre-filtered data by MA to smooth out the noise. For instance, with the V-Q data obtained from $I_t/25$ test with sampling frequency of 0.1 Hz, we firstly smooth the data by using a MA method with a small smoothing window (50 points) to get the outlier of the IC curves, then a Gaussian filter was applied on the curves to smooth out the noises which cannot be eliminated by the simple MA smoothing. The smoothing effect of Gaussian filter is improved by increasing the smoothing window, as illustrated in Fig. 1 (c). This figure compares the IC curves obtained by the proposed method with smoothing window of 50, 100, 200, 300, 500 and 800. Compared to the moving average smoothing method, the GS can offer enhanced smoothing effect. The smoothness of curve can be significantly improved by increasing the Gaussian smoothing window, and all the noise on the differential curves can be effectively filtered by using a smoothing window of 300. These curves after proposed smoothing method under different smoothing windows have high similarities, although the features on curves are also slightly influenced by the width of smoothing window. Too small of the smoothing window cannot provide satisfactory smoothing effect, which can be called under-smoothing. Noise can be clearly seen on the IC curves (in Fig. 1 (c)) when using smoothing window of 50, 100 and 200. When the value increase to 300, the noise can be effectively filtered and the features can be well preserved on IC curves. However, an oversized smoothing window will lead to curve deformation and loss of important information, which is called over-smoothing. This phenomenon can be observed In Fig. 1 (c) with a Gaussian window of larger than 500. When IC curves are over-smoothed, the decrease of the peak intensity and peak shifting to higher voltage levels can be observed. Noted that the increased smoothing window will also increase the computational burden for data processing. Hence, the smoothing window need to be adjusted based on the testing condition before implementing this technique for on-line SoH estimation. A smoothing window of 300 is chosen in this work, as it can provide good smoothing without losing or deforming the important FOIs on IC curves. Fig. 1 (d) compares the IC curves for cell 1 at BoL obtained by the conventional MA method (with smoothing points of 50) with the proposed GS method (with smoothing window of 300). As can be seen, the features of IC curves can be well preserved while the noises are successfully filtered. The positions and heights of the peaks on IC curves can be consequently clearly identified, this is of great significance for accurately correlating the battery SoH with the peak variations during battery ageing in later sections.

The smoothing window in both MA and GS need to be adjusted based on the testing conditions like applied charging/discharging current rate and sampling frequency of data recording. Increased current rate and/or decreased sampling frequency result in reduced amount of data points and the smoothing window should be reduced accordingly in order to preserve the FOIs on IC curves. On the contrary, if lower current rate and/or higher sampling frequency are applied during the experiment, larger smoothing windows need to be used to filter the noise on differential curves.

3.3. Influence of sampling frequency on the IC curves

In the previous research, the voltage sampling frequency used for obtaining V-Q curve varies from one research to another. Han et al. [29] chose 1 Hz as the sampling frequency and they claimed that the battery charged capacity was proportional to the number to sampling points during charging process. Weng et al. [31,40] used a sampling frequency of 10 Hz for the data acquisition. How the sampling frequency can influence the IC curves has not been studied by any of the previous research. The higher the sampling frequency the more data points can be collected during the charging test, however the high sampling frequency will lead to the use of expensive measurement units which in turn affects the total price of the BMS.

Fig. 2 compares the charging IC curves of one cell with different sampling frequency (10 Hz, 1 Hz, 0.1 Hz, 0.2 Hz and 0.01 Hz) with $I_t/2$ current rate. Indeed, more data points can be collected from the test with higher frequency, but it means the derived IC curves are noisier. In this case, we need to increase the smoothing window to get smoothed IC curves. All the important FOIs can be identified regardless of the sampling frequency, however, the peaks are largely deformed when the sampling frequency decreases to 0.2 and 0.01 Hz (see from the enlarged figure of Fig. 2). The curves obtained with 0.2 and 0.01 Hz sampling frequency are quite angular and cannot be further smoothed due to lacking of sampling data. At such low sampling frequency, the peaks shift toward to the higher voltage level and the intensity of peaks decrease significantly. The IC curves achieved with sampling frequency of

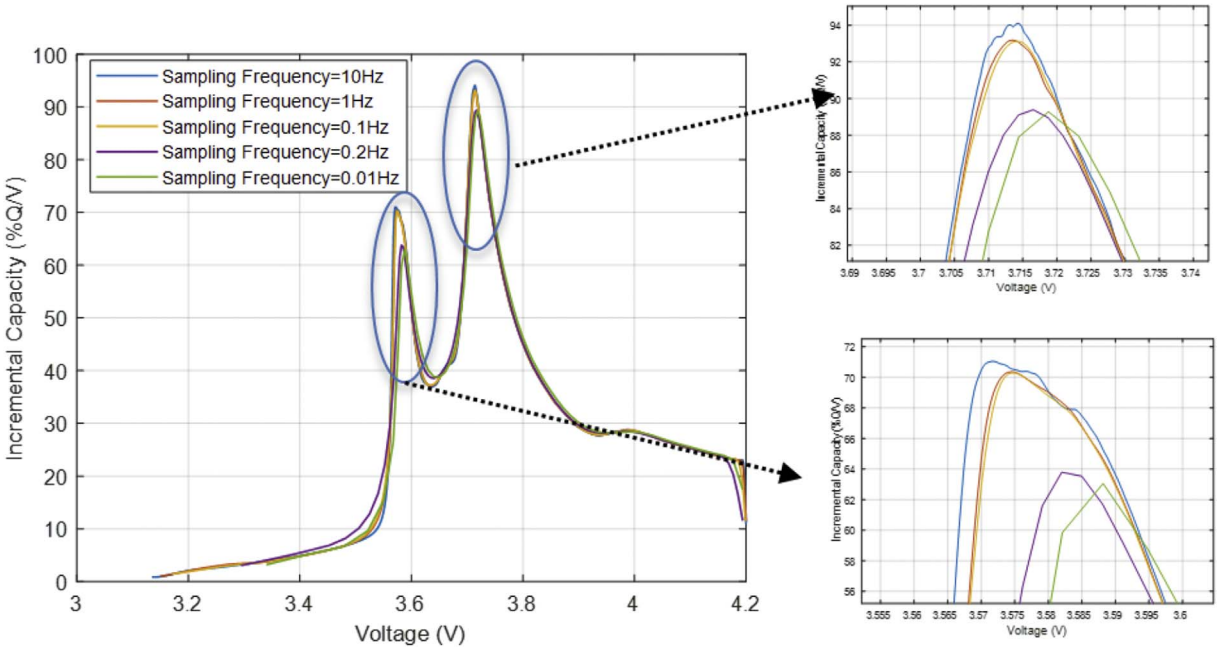

Fig. 2. Comparison of IC curves with different sampling frequency under current rate of $I_t/2$.

10 Hz, 1 Hz and 0.1 Hz are almost identical, increasing sampling frequency is therefore not helpful for gaining extra information from the IC curves.

The testing sampling frequency should be controlled in an appropriate range. Increasing the sampling frequency requires augmented computational effort for data processing and also increases the BMS cost of data recording. On the other hand, if the sampling frequency is too low, the derived IC curves will lose their fidelity of SoH identification as the peak position and intensity are largely changed. In this work, we choose 0.1 Hz as the sampling frequency as it can provide enough useful data points for deriving IC curves as well as decreased the computational effort of curve smoothing.

4. Battery degradation mechanism identification

4.1. Previous research on ageing mechanism of NMC batteries

Ageing is a phenomenon which leads to loss of capacity or increase in internal resistance in Li-ion batteries during both cycling and storage and it occurs due to various side reactions inside the cell [41]. According to the previous research, the ageing mechanisms for Li-ion cells can be categorized into the following groups: (1) loss of lithium inventory (LLI), (2) loss of active material (LAM) and (3) resistance increase (RI) [42].

LLI is mainly related to solid electrolyte interphase (SEI) formation and side reactions caused by decomposed electrolyte [42]. It has been well established that dominant ageing mechanisms on graphite anodes are caused by SEI formation, which can also result in a significant increase of the impedance and a limitation of the electrode kinetics [43]. LAM can directly affect the usable capacity of the electrodes and originates from three basic conditions: structural changes during cycling, chemical decomposition or dissolution reactions of transition metal into the electrolyte solution and surface film modification [42,44]. LAM can be further categorized as four different modes: LAM on the positive electrode (PE) in the lithiated/delithiated state (LAM_{liPE}/LAM_{dePE}), LAM on the negative electrode (NE) in the lithiated/delithiated state (LAM_{liNE}/LAM_{deNE}) [3]. RI is the result of the degradation on both the electrodes and electrolyte and both LAM and LLI can contribute to RI [42].

To date, the research on ageing mechanism identification of NMC containing Li-ion batteries with graphite as negative electrode has been done on laboratory cell scale as well on the commercial cell scale [30,44–46]. The research done on laboratory scale, used manually assembled cells in laboratory pouch cells or coin cells as research objects. For instance, Zeng et al. [45] performed a post-mortem analysis on the NMC/graphite battery after cycling and found that LAM happened on the PE due to the destruction of structure and decreased the diffusion rate of Li ions moving in/out of PE. The test result from Buchberger et al. [47] on NMC cells indicates that LLI is the mainly cause for capacity fade during cycling ageing and LAM is found to be the main ageing mechanism when cells are over-charged. Bloom et al. [30] conducted DV analysis on NMC cells and found that the battery capacity fade is mainly caused by the side reactions at the negative electrode. It was reported by Sarre et al. [48] that impurities, manufacturing processes, and cell design play a role in the aging reaction rates. This is further confirmed by the research of Niehoff et al. [49] after comparing the ageing results of hand-assembled 40 mAh cells and automatically manufactured 40 A h cells, consisting of same materials. Stiaszny et al. [46] investigated the calendaring ageing mechanism of commercial 18650-type Li-ion batteries with $LiMn_2O_4/Li(Ni_{0.5}Co_{0.2}Mn_{0.3})O_2$ as PE and graphite as negative electrode (NE) at elevated temperature. They detected that the capacity fade was mainly caused by LLI due to SEI layer growth, a small portion of LAM on PE due to formation of isolated particles and transition metal dissolution was believed to contribute to the total capacity fade. They also found that RI happened due to electrolyte decomposition and diffusion limitation inside the electrodes. Dubarry et al. [50] investigated the effects of temperatures on the ageing behaviors of cycled 18650-type batteries with $Li_xMn_2O_4/Li(Ni_{1/3}Co_{1/3}Mn_{1/3})O_2$ blend as PE and graphite as NE. They found that LAM, SEI formation and the hindrance to kinetics are the main reasons for causing the battery capacity fade at high temperatures. The study on ageing mechanism detection for large commercial cells was performed by Jalkanen et al. [44], they found SEI layer growth and lithium plating are the main contributions to battery capacity loss during cycling, while no signs of structural/chemical changes in the active material from both electrodes were found in the aged cells. They also observed a significant increase of both ohmic and polarization resistance because of electrolyte consumption and possible blockage of separator pores. The overview of previous research on the NMC battery ageing process shows that the capacity and power fade are

not caused by one single factor, but from a number of various processes and their interactions. Various impact factors influence synthetically on the ageing processes and complicate the investigation of ageing mechanisms. The studies of ageing mechanisms in large-scale pouch cells are still scarce and a better understanding of their degradation process will enable researchers to develop more accurate SoH estimation models. Therefore, it's necessary and important to carry out research on the ageing path of the objective high NMC batteries under the specific cycling conditions.

4.2. Ageing mechanism of high energy NMC batteries

Herein, we use the IC analysis with a very low current rate ($I_t/25$) to acquire more information of the aging mechanism associated with the cycling of this cell. At such low current rate, the polarization influence on the IC curves can be decreased, and the shape of the curve will be as detailed as possible [51]. The charging voltage curves of cell 1 from the capacity test under current rate of $I_t/25$ at different ageing states are shown in Fig. 3(a). The charge voltage slightly shifts toward to the lower capacity level during cycling due to battery capacity loss. Two clear voltage plateaus can be identified from the V-Q curves due to phase changes during charging, which are pointed out by the blue circles. The information about the battery ageing mechanism is contained in the shift of voltage plateaus. By applying IC analysis, these voltage plateaus can be transformed into peaks, and the specific degradation mechanism can be distinguished by analyzing the progression of each peak in IC curves throughout ageing.

In Fig. 3 (b), the charging IC curves of cell 1 after different cycling numbers are compared. Five different feature of interests (FOIs) are observed on the IC curves, marked as A, B, C, D and E. A and B are peaks have their initial maximum of intensity at 3.47 V and 3.60 V, respectively. C is considered as the shoulder of this IC curve, which starts from 3.83 V. E is the valley between peak A and B, located around 3.60 V. The valley D is located around 3.80 V, which is a valley between peak B and shoulder C. According to the previous research, peak A is mainly influenced by the reactions on the negative electrode [27,52–54], and peak B might be dominated by the sequential phase transition process $Ni^{2+} \rightarrow Ni^{3+} \rightarrow Ni^{4+}$ in NMC cathode [27,52–56]. The area under each peak represents the capacity of the related reaction during the cycling process [57]. The FOIs will be further used as features of interest for analysis, the change of their intensity and positions will be recorded to collect the information about cell degradation mechanisms.

The variation of peak intensity and location of peak A and B along with ageing are illustrated in Fig. 3 (c). The intensity of peak A is decreasing slightly from 0 till 700 cycles and then increasing from 700 to 1000 cycles. Nevertheless, the variation of peak A's intensity is relatively small (less than 5%) during ageing. The intensity of peak B is decreasing with the battery ageing state, dropping 20% compared with the original peak intensity after 1000 cycles. It should be noticed that even though the intensity of peak B is decreasing, the width of the peak is increasing, which can be explained by the deteriorating kinetics [53]. Despite the evolution in peak intensity, the positions of all peaks on IC curves were simultaneously shifted toward a higher voltage level, while the positions on DV curves remain unchanged on DV curves during battery ageing. The increase of resistance inside of battery can contribute to this phenomenon according to the previous research of Ref. [22,24]. Noted that lower anode potential can also leads to the peak shifting, which might be resulted from lithium plating. The exact degradation process needs to be confirmed a post-mortem analysis.

To identify LAM on positive electrode, DV curves can be used to investigate the battery internal changes during their ageing. The DV curves of cell 1 during charging process after different cycling numbers are shown in Fig. 3 (d). The valleys D and E in IC curves are corresponding to the peaks P_D and P_E on DV curves, respectively. It should be noted that the areas underneath the peaks in IC curve, marked by [baseline = (char.base)] [shape = circle, draw, inner sep = 1.5 pt] (char) 1; , [baseline = (char.base)] [shape = circle, draw, inner sep = 1.5 pt] (char) 2; and [baseline = (char.base)] [shape = circle, draw, inner sep = 1.5 pt] (char) 3; in Fig. 3 (b), can be simply identified by measuring the width of section Q_a, Q_b and Q_c in DV curves (shown in Fig. 3 (d)). These peak areas represent the capacity involved in the related reaction in this region. All the DV curves have a very similar shape in region Q_a and Q_b regardless the cell age, an obvious reduction of Q_b can be seen along with battery ageing. Fig. 3 (e) demonstrates the variation of section Q_a, Q_b and Q_c with cycling number, the values of Q_a and Q_b remain almost unchanged while Q_c decreases largely during battery ageing.

Area [baseline = (char.base)] [shape = circle, draw, inner sep = 1.5 pt] (char) 1; is composed of the areas under peak A and E in Fig. 3 (b)). The intensities of both peaks remain almost invariant and therefore the value of region Q_a is unchanged during aging. It should be mentioned the area under peak B is defined as the region between valley E and valley D. During battery ageing, valley D is shifting to higher voltage level, which leads to the expanding of bottom width of peak B (marked by the red arrow in Fig. 3 (b)). The decreased area at the top of peak B is compensated by the enlarged area at the bottom part. This explains why the total area [baseline = (char.base)] [shape = circle, draw, inner sep = 1.5 pt] (char) 2; can stay unchanged, which is reflected by the unvaried value of Q_b on DV curves of Fig. 3 (d). The reduction of shoulder C's intensity and bottom width indicate the decline of this peak area, which can also be identified from the decreased value of Q_c on DV curves from Fig. 3 (e). The width of Q_a and Q_b stay almost unchanged, indicating no obvious LAM on anode material during ageing [58]. Whether LAM happens on positive material during ageing cannot be identified from the full cell IC analysis. The decrease of Q_c indicates LLI is the main cause for battery capacity loss [28,55,58]. Nevertheless, post-mortem analysis is required to precisely detect the degradation mechanism.

5. On-line SoH estimation based on positions of FOIs

5.1. Improved SoH estimation method with decreased testing time

Based on the ageing mechanism analysis on the tested batteries, we could relate the variation of FOIs to the battery capacity fading process and therefore identify the battery SoH. Monotonic trends in the positions of FOIs can be clearly identified on IC curves as battery ages. The peaks on DV curves stay almost unchanged during the ageing process, it is therefore difficult to correlate the capacity fade with the location and intensity of peaks on DV curves and makes them unsuitable for online SoH identification. Additionally, batteries for on-line application are charged from different SoC levels, and it leads to large changes of peak positions on DV curves due to the variation of charging capacity. Nevertheless, the peak positions on IC curves will not be influenced by partial charging since the voltage of a battery has a definite position [57]. Hence, IC curves are more suitable for online SoH estimation than DV curves.

The charging or discharging at the current rate of $I_t/25$ requires too much time in real application (approximately 50 h to finish the charge and discharge steps). In order to find the best and the quickest solution that has a good compromise between test time and accuracy, different current rates at charging processes were evaluated. Fig. 4 shows the IC curves obtained from constant charge steps under different current rates: $I_t/25$, $I_t/3$, $I_t/2$ and $1I_t$. The potential shift of the IC peaks with a different current rate is caused by the polarization effect [24]. When cells are charged under $1I_t$, no clear shoulder C and valley D can be identified from the IC curves, accordingly we chose the IC curves with $I_t/2$ for further research on battery SoH estimation as it was the largest current rate that enabled of observing all the four FOIs of IC curves for this type of cells and the test time can be largely decreased.

Fig. 5 (a) shows the IC curves of cell 1 obtained during charging at

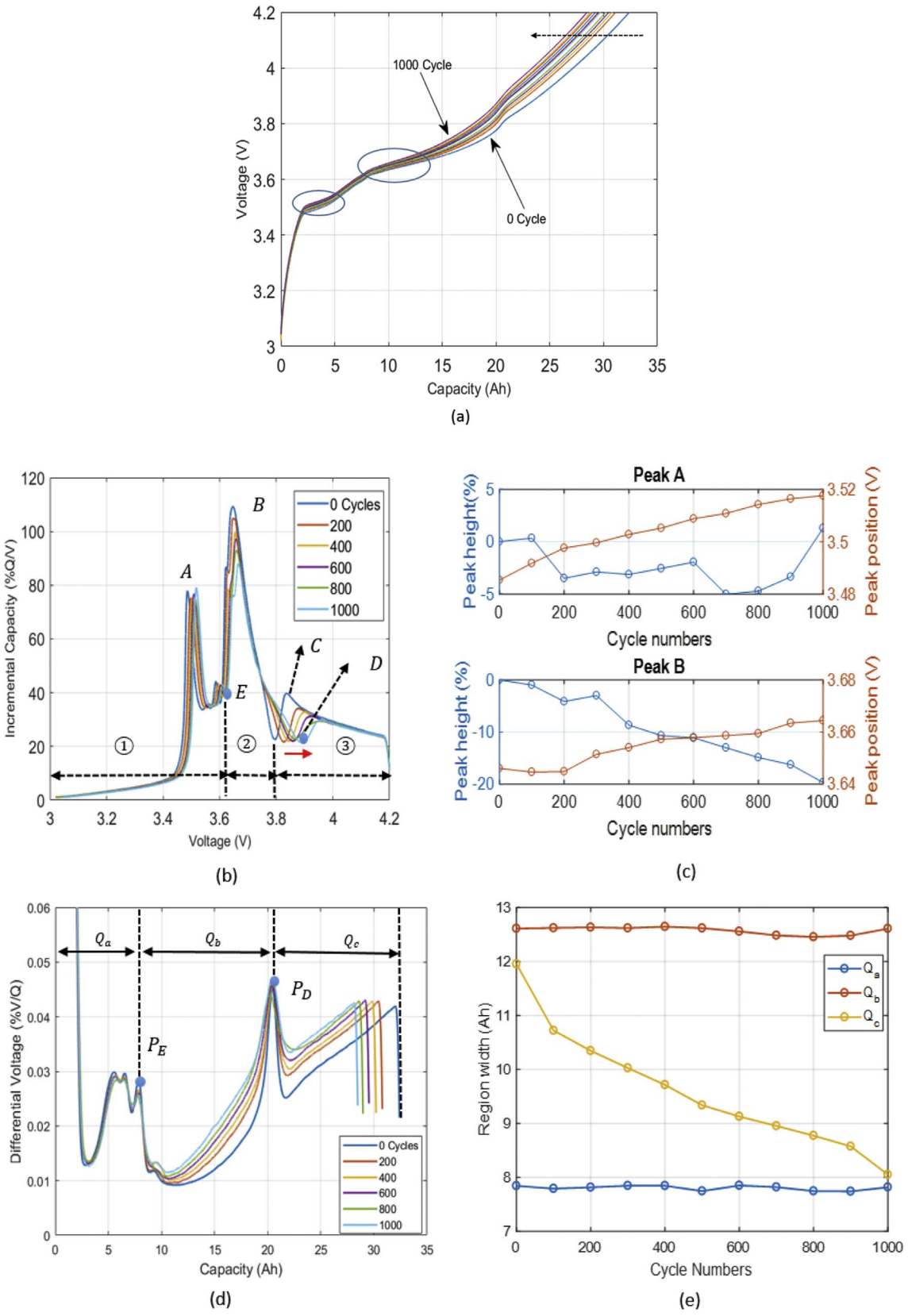

Fig. 3. (a)An illustration of voltage-capacity curves during charging process with current rate of $I_t/25$ after different cycles, (b) representative charging IC curves at different ageing states, (c) variation of the height and position of peak A and B on IC curves, (d) representative charging DV curves at different ageing states, (e) evolution of region width on DV curves.

different ageing states with $I_t/2$. As mentioned in Section 3.2 that the smoothing window need to be adjusted based on the applied current rate. Herein, a MA smoothing window of 50 with a Gaussian smoothing window 30 are used for processing the IC curves. The shapes of all the IC curves are very similar, this allows to identify the battery SoH by tracking the location and intensity change of the four FOIs. However,

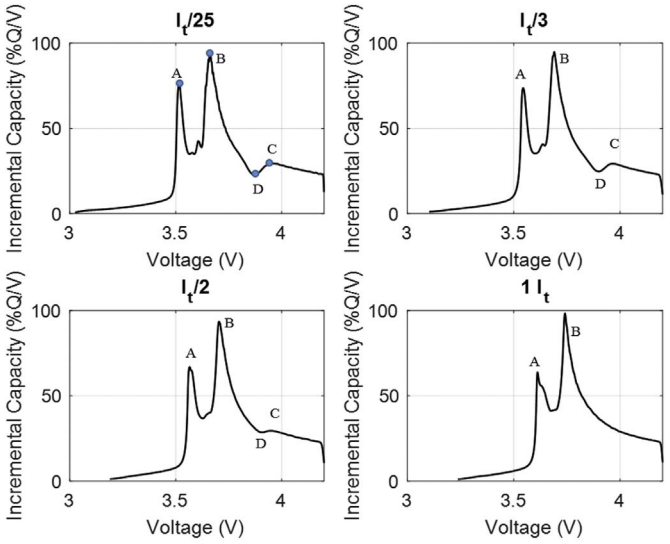

Fig. 4. Charge IC curves for cell 1 under different discharge current rate of $I_t/25$, $I_t/3$, $I_t/2$ and $1I_t$.

the intensity of shoulder C is decreasing as battery ages and it will be difficult to identify after a certain number of cycles. Hence, we choose valley D as indicator instead of shoulder C, as D can be easily measured by identifying the point where the IC curve slope is equal to zero in the voltage region of 3.8 V–4 V.

The variations of the positions and intensity of peak A, B and valley D are illustrated in Fig. 5 (b). The intensity of peak A and B are decreasing with cycling, but no clear correlation between cycling numbers with intensity of valley D was identified. Nevertheless, all the positions of the peaks and valley are shifting towards to higher voltage level, and the positions of FOIs are thereby selected for further study. Having detected these characteristics of IC curves, it is promising to estimate the battery SoH based on the detection and measurement of the location of the three FOIs.

The battery SoH is plotted versus the location of peak A, B and valley D, which are illustrated in Fig. 5 (c) and (d). The monotonic characteristic of position as batteries degrade has been verified through the IC curve analysis, and a linear regression function between battery SoH and all three FOIs can be established with Eq. (5).

$$SoH_{FOI} = \alpha_{FOI} - \beta_{FOI} \times P_{FOI} \tag{5}$$

where P_{FOI} represents the identified positions of FOIs on the IC curve

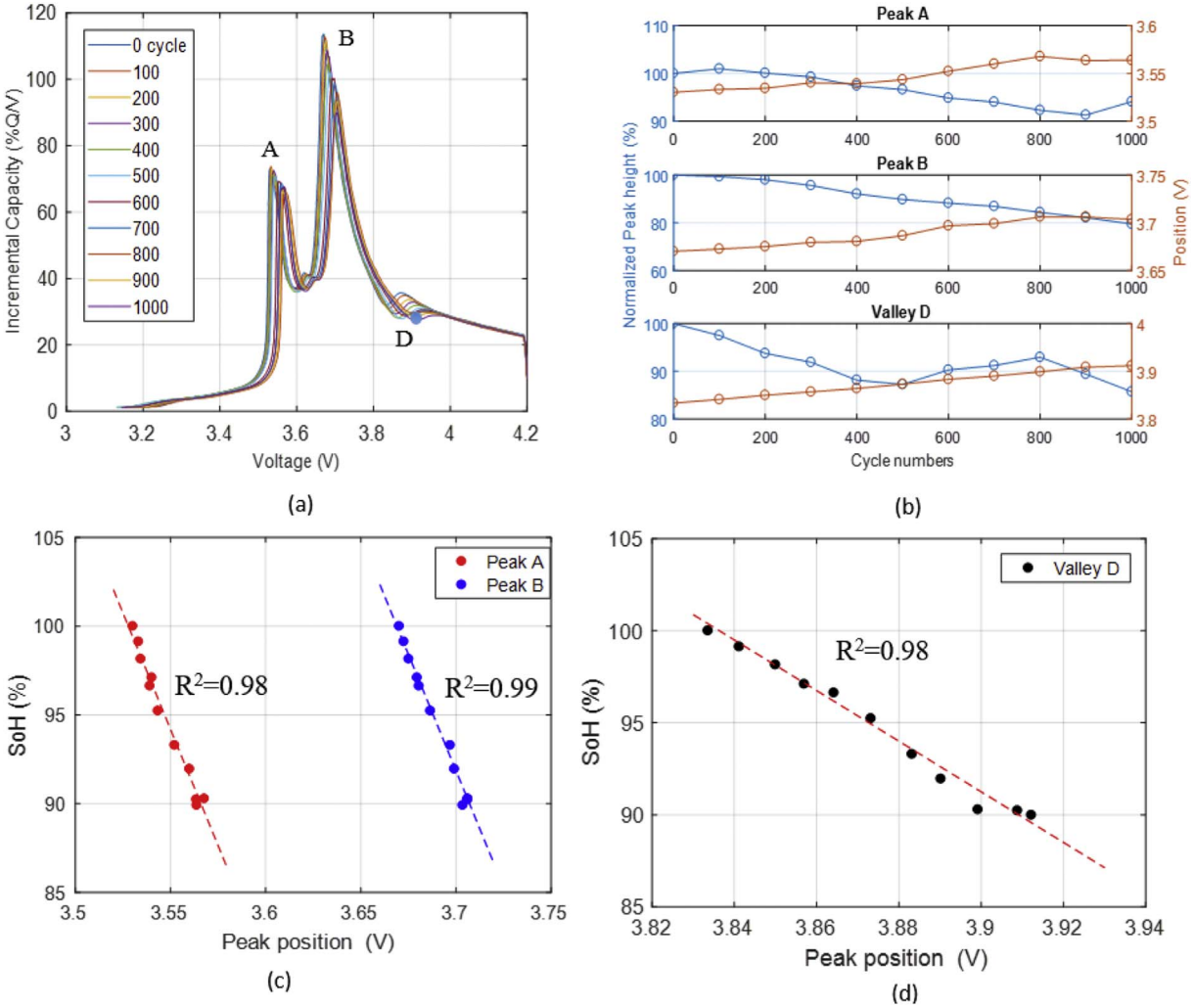

Fig. 5. (a) Charge IC curves for cell 1 at BoL under $I_t/2$ after different cycles (b) variation of positions and intensity of FOIs on IC curves during ageing (c) the battery SoH as function of the position of peak A, B (d) the battery SoH as function of the position of valley D.

Table 3
Coefficients for SoH estimation function with different FOIs.

FOIs	α_{FOI}	β_{FOI}
Peak A	1025	262.2
Peak B	1062	262.2
Valley D	503.1	105.4

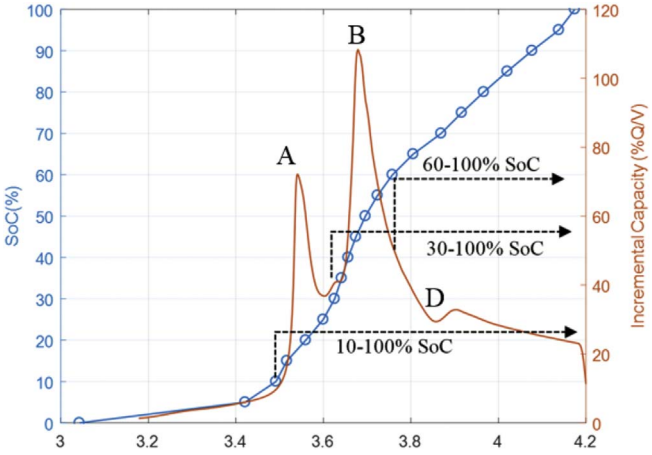

Fig. 6. Illustration of IC curve with OCV curve during charging process at BoL.

with unit V, SoH_{FOI} is the estimated SoH with the chosen FOI, α_{FOI} and β_{FOI} are the empirical coefficients determined by using the Matlab curve fitting toolbox. The specific values of α_{FOI} and β_{FOI} for tested cell 1 are listed in Table 3. As three signatures of the curve located at different voltage levels (peak A, B and valley D) can well correlate with the battery capacity, all of them can be therefore used for SoH estimation. This allows identifying battery SoH with partial charging data and flexible initial charging SoC levels. It should be noted that these functions are derived from the charging voltage curves with current rate of $I_t/2$, the coefficient of the functions need to be adjusted if a different charging current rate is applied. IC analysis is shown to be a useful tool for battery SoH assessment.

5.2. SoH estimation with partial charging

It is rarely to fully discharge the batteries in real applications and start charging from 0% SoC, instead, they are normally charged from an uncertain SoC point. Thus, the developed SoH estimation method should be able to utilize partial charging curves. Fig. 6 illustrates the IC curve and the open circuit voltage (OCV) curves of cell 1 during charging process at BoL, the corresponding SoC regions of IC peaks can be easily identified from the OCV curves. In order to identify peak A, the starting charging SoC of battery should be no more than 10%. To derive peak B, the starting charging SoC should be lower than 30% and the starting SoC level should be less than 60% in order to get valley D.

Fig. 7 illustrates the correlation between the SoH of the six batteries with the position of FOIs by fitting the proposed linear equation in Eq. (5). The V-Q curves during cycling ageing test are used to derive IC curves. For cell 1 and 2, all three FOIs can be identified as they are cycled from 0% to 100% SoC. For cell 3 and 4, the starting charging SoC level of 20% is lower than 30% but higher than 10%, only two FOIs (peak B and valley D) can be seen. For cell 5 and 6, the starting charging SoC 40% is lower than 60% but higher than 30%, which only allows for the identification of one FOI (valley D). As can be seen, the developed linear equation from cell 1 can also be well fitted for the other cells which are cycled under the same (cell 2) and different (cell 3, 4, 5 and 6) cycling conditions with less than maximum 2.5% estimation errors. The small estimation errors prove the robustness and generality of this method. This method is applicable for the cells under partial charging process and therefore the testing time is largely reduced.

With the established linear correlation function between the battery SoH and the position of FOIs, an on-line SoH monitoring framework can be established. The proposed multi-stage SoH identification method for this type of NMC batteries during static charging process is shown in Fig. 8. The initial charging SoC level for the batteries need to be identified before SoH estimation to see if it is possible to get FOIs from the static charging curve. The maximum threshold of SoC for identifying battery SoH is 60%, the battery need to be discharged first if the initial SoC is higher than this value. If the cell is charged from an initial SoC level of lower than 10%, all the FOIs can be found on the IC curves, and the value of position of peak A, B and valley D can be used for battery SoH estimation by using Eq. (5). If the initial charging SoC level is in the range of 10%~30%, peak B and valley D can be recognized from the IC curves, two estimated SoH values will be obtained with the two FOIs. When the initial charging SoC of the cell is in the range of 30%~60%, only valley D can be seen on the IC curve and therefore the estimated SoH value can be calculated based on one FOI. When multiple FOIs are acquired from IC curve, the average value can be calculated for indicating the battery SoH. This method also shows its adaptability in the cases when batteries are not fully charged to 100% SoC, as the SoH can be estimated as long as one of the three FOIs can be identified from the IC curves. For instance, if the batteries are charged from 10% SoC to 30% SoC, Peak A can be observed from the curve even though peak B and valley D are missing. With the position of Peak A, the real-time battery SoH can still be estimated.

The whole on-line SoH estimation process can be summarized as the following steps:

- Obtaining V-Q curve: before starting the SoH estimation step, the initial battery SoC need to be checked to ensure it is in the range of 0%~60%, then the cells can be charged to the cut-off voltage.
- Deriving IC curve: the charging V-Q curves are used to obtain IC curve with numerical derivative method and the IC curves are smoothed with the proposed GS method.
- Estimating SoH: the positions of the FOIs can be measured from smoothed IC curves and the battery SoH is then estimated by using the established linear function in Eq. (5).

With this proposed method, the online SoH identification for battery can be achieved with partial charging data, it can be run on a daily basis during static charging process.

5.3. Validation

For the validation of the proposed multi-stage SoH estimation method, partial charging tests with different starting SoC levels (10%, 15%, 20%, 25%, 30%, 50% and 60%) were conducted on the cells at different SoH. The estimated SoH results were compared with the tested capacity value obtained from the $I_t/3$ capacity test to calculate the estimation error. To assist the comprehension of validation process, the estimation results from three cells (Cell 1, 3 and 5) aged under different cycling depth were used as examples to prove the robustness of the proposed method.

The cells were charged from different starting SoC points with current rate of $I_t/2$, the partial charging curves were used to derive IC curves and the positions of FOIs can be easily identified by following the testing steps in Fig. 8. With the information of FOIs locations on the IC curves, the battery SoH can be estimated. The result of locations of FOIs, the corresponding estimated SoH and errors are listed in Table 4. Different initial charging SoC points lead to different amount of identifiable FOIs on the IC curves. Take cell 3 as an example, the real capacity was obtained with the capacity test profile and a SoH of 88.9% was calculated as the real SoH value for reference. When cell 3 was

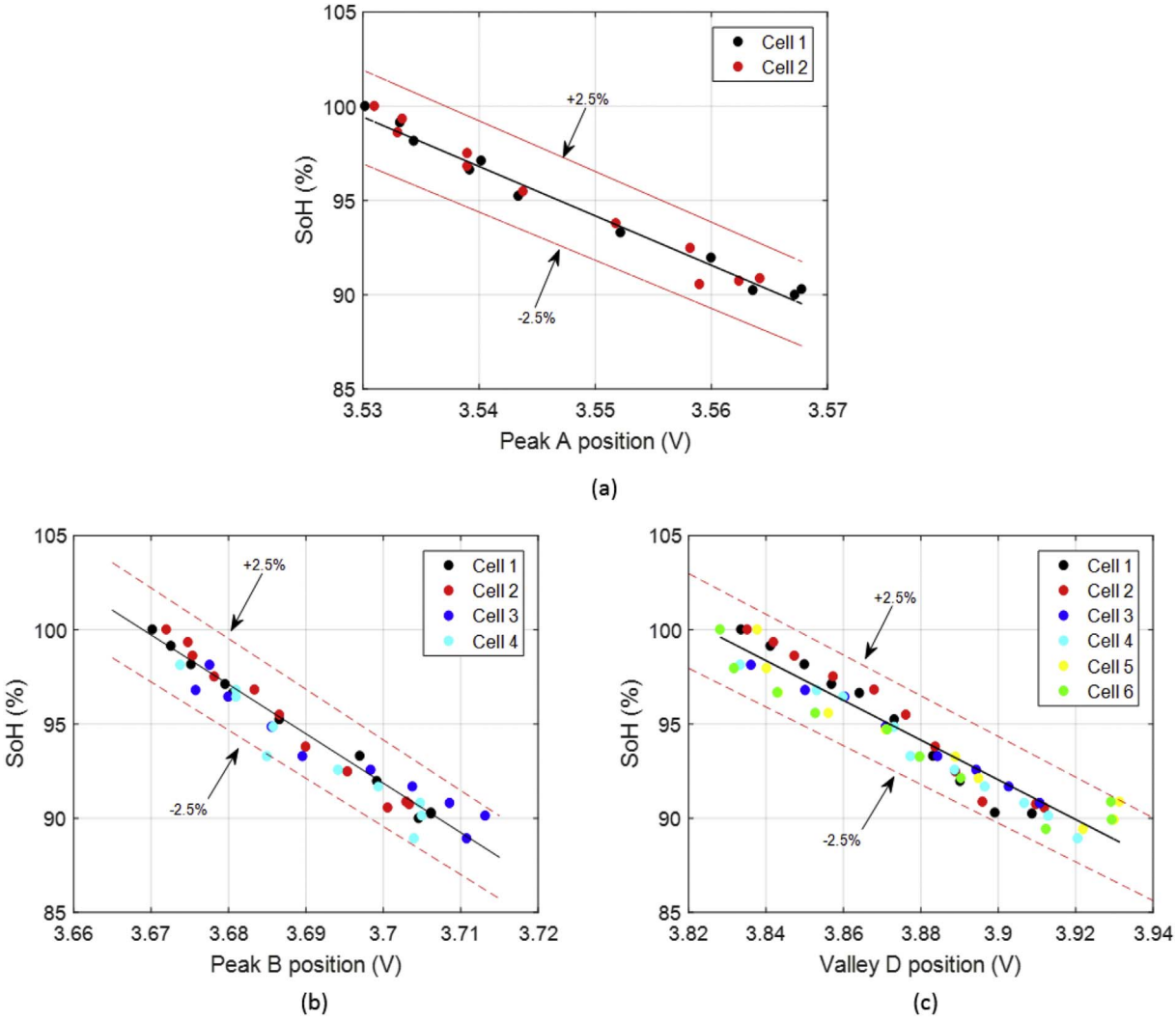

Fig. 7. Correlation between battery SoH and the position of (a) peak A (b) peak B and (c) valley D for all tested cells from life cycle ageing test.

charged from 20% SoC with current rate of $I_t/2$, Peak B and valley D can be identified from the IC curve, two SoH values of 89.47% and 88.75% can be calculated based on the positions of the two FOIs, respectively. By calculating the absolute difference between both the real and estimated SoH values, an error of 0.21% was obtained if the value of peak B's position was used for SoH estimation and an error of 0.43% by using the value of valley D's position. For the final indication of battery SoH, the average SoH value of 89.11% can be used with estimation error of 0.24%. When the initial SoC is 50%, only the position of valley D can be used for estimating SoH. This derives an estimated SoH of 89.62% with an absolute estimation error of 0.82%.

The less than 2.5% maximum absolute estimation errors prove the robustness of this multi-stage SoH estimation method. With the proposed multi-stage SoH estimation method, the battery can be charged from different SoC levels. The maximum allowable SoC level for starting charging the battery is 60%, which fits most application cases of batteries. With the enhanced charging current rate of $I_t/2$ and the allowable partial charging condition, the testing time for SoH estimation can be reduced to minimum 0.8 h when the cells are charged fully. The time required for battery SoH estimation with different initial charging SoC can also be found in Table 4.

To summarize, an on-line SoH monitoring framework is developed in this work by constructing quantitative correlations between the battery capacity with the positions of FOIs on IC curves. Gaussian filter is applied in combination with the moving average method to smooth the IC/DV curve. This advanced smoothing method can largely improves the quality of derived IC curves compare with the curves obtained from conventional MA method. The noise on the derived IC curves can be completely filtered without changing the properties of FOIs on IC curves and the information related to battery capacity fade from the FOIs can be therefore accurately extracted. Three FOIs (peak A, B and valley D) in IC curves were chosen as indicators for battery SoH estimation based on their positions. Given that all the three FOIs at different voltage levels are shifting towards to a higher voltage level as the battery ages, a multi-stage SoH estimation method is proposed. It utilizes partially charging data with a maximum SoC threshold of 60%, which can cover most cases for battery charging during real-time operations. Six high energy NMC batteries cycled under different conditions are used to validate the proposed method. The results show that the linear function developed between FOIs position versus battery SoH from cell 1 can evaluate the SoH of the other five cells which are cycled under the same (cell 2) and different (cell 3, 4, 5 and 6) cycling conditions. The less than 2.5% maximum estimation errors prove the robustness of this method. This proposed IC based SoH monitoring framework could be used on a daily bases and fully charging/discharging data is only needed for SoH calibration after a certain period of operation. The proposed on-line SoH estimation method requires a charging current rate ($I_t/2$), it also shows potential for being applied in the cases with faster charging current rates. When the current rate largely increases, some of the FOIs will disappear and therefore make it

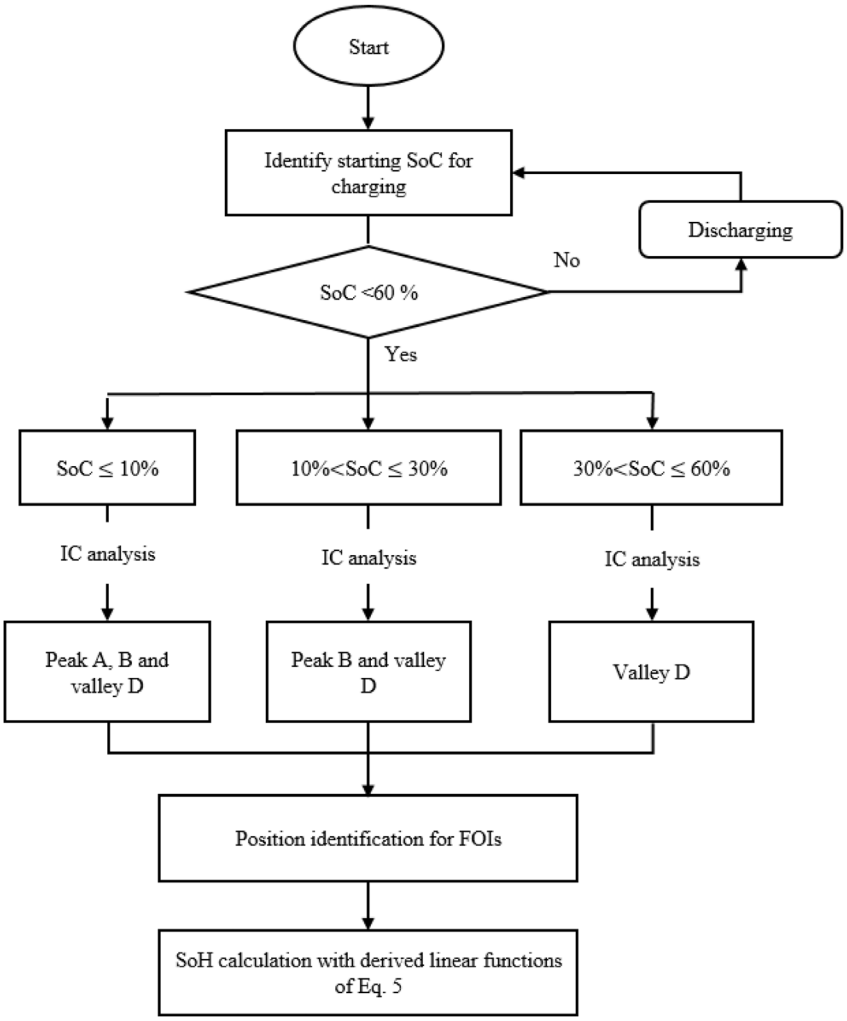

Fig. 8. Flowchart of multi-stage SoH identification method.

impossible to have multi-stage SoH estimation. Nevertheless, the main peak B can still be detected and it can be used as the indicator for battery SoH. Which current rate should be applied for on-line SoH estimation is depending on the requirements of specific application.

5.4. Future work

The most desirable SoH estimation tool for lithium ion batteries lies in the simplicity, generality and accuracy for any kind of batteries. Taking into account that the battery performances are influenced by many other factors like chemistry, cell design, battery geometry, working conditions (e.g. temperature and cycling current rate) and manufacturing process. It is of significance and necessity to carry out ageing test by considering the aforementioned impact factors in the future work. At moment, only single cells are being studied for the ageing mechanism and SoH estimation. In realities, cells are connected in series and/or parallel to form battery pack. Given the fact that the inherent variations exist among the cells in a battery pack due to manufacturing process and in-homogeneous operating conditions and the cell-to-cell variation will become even larger when the cells age. These variances result in SoH deviation among individual cells in the battery pack, therefore, the SoH estimation method for single cell may not be suitable for the whole battery pack. How to adapt the SoH estimation technique based on IC peak tracking from cell level to multi-cell module level remains an open question, which will be discussed in the following work.

6. Conclusion

In this paper, we developed a battery SoH estimation tool with specific emphasis on utilizing partially charging data for on-line implementation. A new smoothing method based on Gaussian filter is introduced to derive IC/DV curves and its basic principles are introduced. With the proposed smoothing algorithm, an SoH estimation framework is developed to provide a quantitative correlation between positions of FOIs on IC curves with battery capacity fade. The battery SoH can thereby be estimated from normal charging data with flexible initial charging SoCs during real-life operation. The obtained results are accurate and precise with maximum 2.5% estimation error. This technique shows good characteristics of providing accurate estimation results and moderate computational effort. It only requires the static charging voltage-capacity curve and shows good potential for the implementation in a BMS.

The battery degradation mechanism is also shortly discussed in this paper by analyzing the evolution of the FOIs on IC/DV curves under low current of $I_t/25$. We could decipher the main contribution to the capacity fading of this commercial NMC cell, which is caused by LLI. A small portion of LAM is suspected to happen on positive materials. Nevertheless, the exact ageing mechanism of the tested batteries need to be confirmed by post-mortem analysis in the future work. As the variations of FOIs on IC curves are more related of LLI, further studies are need to verify the applicability of the developed SoH estimation methodology to another ageing mechanism.

Table 4
Battery SoH estimation results from three different cells.

Cell No.	Real SoH (%)	FOIs		Initial charging SoC (%)						
				10	15	20	25	30	50	60
1	90.4	Peak A	Position(V)	3.56	–	–	–	–	–	–
			Estimated SoH (%)	92.16	–	–	–	–	–	–
			Estimation error (%)	1.95	–	–	–	–	–	–
		Peak B	Position(V)	3.708	3.700	3.700	3.709	3.706	–	–
			Estimated SoH (%)	89.7	91.8	91.8	90.8	90.18	–	–
			Estimation error (%)	0.74	1.59	1.59	0.47	0.239	–	–
		Valley D	Position (V)	3.915	3.915	3.913	3.908	3.908	3.904	3.899
			Estimated SoH (%)	90.49	90.60	90.67	91.22	91.20	91.36	92.05
			Estimation error (%)	0.10	0.22	0.29	0.9	0.88	1.07	1.83
		Average estimated SoH (%)		90.78	91.2	91.23	91.01	90.69	91.36	92.05
		Absolute estimation error (%)		0.42	0.88	0.92	0.67	0.32	1.07	1.83
3	88.9	Peak A	Position(V)	3.565	–	–	–	–	–	–
			Estimated SoH (%)	90.2	–	–	–	–	–	–
			Estimation error (%)	1.46	–	–	–	–	–	–
		Peak B	Position(V)	3.709	3.708	3.709	3.712	3.715	–	–
			Estimated SoH (%)	89.4	89.73	89.47	88.71	87.88	–	–
			Estimation error (%)	0.58	0.93	0.64	0.21	1.14	–	–
		Valley D	Position (V)	3.934	3.932	3.931	3.926	3.926	3.923	3.918
			Estimated SoH (%)	88.4	88.6	88.75	89.29	89.63	89.62	90.11
			Estimation error (%)	0.52	0.33	0.16	0.43	0.82	0.81	1.37
		Average estimated SoH (%)		89.33	89.16	89.11	89.00	88.75	89.62	90.11
		Absolute estimation error (%)		0.49	0.30	0.24	0.11	0.16	0.81	1.37
5	87.9	Peak A	Position (V)	3.566	–	–	–	–	–	–
			Estimated SoH (%)	89.98	–	–	–	–	–	–
			Estimation error (%)	2.36	–	–	–	–	–	–
		Peak B	Position (V)	3.708	3.706	3.707	3.709	3.714	–	–
			Estimated SoH (%)	89.55	90.1	90.06	89.31	88.29	–	–
			Estimation error (%)	1.88	2.5	2.45	1.606	0.44	–	–
		Valley D	Position (V)	3.94	3.939	3.935	3.932	3.925	3.928	3.918
			Estimated SoH (%)	87.7	87.90	88.33	88.64	89.26	89.10	90.10
			Estimation error (%)	0.22	0.01	0.48	0.84	1.54	1.37	2.5
		Average Estimated SoH(%)		89.08	89.00	89.20	88.98	88.78	89.62	90.11
		Average Estimation Error(%)		1.34	1.26	1.48	1.22	0.99	0.81	1.37
Required Testing Time (h)				1.8	1.7	1.6	1.5	1.4	1	0.8

Acknowledgment

This research work is funded by ENGIE Laborelec. We acknowledge the support to our research team from 'Flanders Make'. The authors would like to thank Yang Gao from National Active Distribution Network Technology Research Center (NANTEC), Beijing Jiaotong University for very fruitful discussions. We also thank Xinhua Gao, Dr. Joris Jaguemont and Dr. Jelle Smekens from Vrije Universiteit Brussel for the valuable feedback regarding this work.

References

[1] B. Diouf, R. Pode, Potential of lithium-ion batteries in renewable energy, Renew. Energy 76 (2015) 375–380.
[2] T. Xu, W. Wang, M.L. Gordin, D. Wang, D. Choi, Lithium-ion batteries for stationary energy storage, JOM J. Minerals, Metals Mater. Soc. 62 (9) (2010) 24–30.
[3] M. Dubarry, M. Berecibar, A. Devie, D. Anseán, N. Omar, I. Villarreal, State of health battery estimator enabling degradation diagnosis: model and algorithm description, J. Power Sources 360 (2017) 59–69.
[4] L. Wang, C. Pan, L. Liu, Y. Cheng, X. Zhao, On-board state of health estimation of $LiFePO_4$ battery pack through differential voltage analysis, Appl. Energy 168 (2016) 465–472.
[5] M. Berecibar, I. Gandiaga, I. Villarreal, N. Omar, J. Van Mierlo, P. Van den Bossche, Critical review of state of health estimation methods of Li-ion batteries for real applications, Renew. Sustain. Energy Rev. 56 (2016) 572–587.
[6] M. Berecibar, M. Garmendia, I. Gandiaga, J. Crego, I. Villarreal, State of health estimation algorithm of $LiFePO_4$ battery packs based on differential voltage curves for battery management system application, Energy 103 (2016) 784–796.
[7] N. Omar, J. Van Mierlo, B. Verbrugge, P. Van den Bossche, Power and life enhancement of battery-electrical double layer capacitor for hybrid electric and charge-depleting plug-in vehicle applications, Electrochimica Acta 55 (25) (2010) 7524–7531.
[8] C.T. Love, M.B. Virji, R.E. Rocheleau, K.E. Swider-Lyons, State-of-health monitoring of 18650 4s packs with a single-point impedance diagnostic, J. Power Sources 266 (2014) 512–519.
[9] M. Galeotti, L. Cinà, C. Giammanco, S. Cordiner, A. Di Carlo, Performance analysis and SOH (state of health) evaluation of lithium polymer batteries through electrochemical impedance spectroscopy, Energy 89 (2015) 678–686.
[10] D. Andre, C. Appel, T. Soczka-Guth, D.U. Sauer, Advanced mathematical methods of SOC and SOH estimation for lithium-ion batteries, J. Power Sources 224 (2013) 20–27.
[11] J. Remmlinger, M. Buchholz, T. Soczka-Guth, K. Dietmayer, On-board state-of-health monitoring of lithium-ion batteries using linear parameter-varying models, J. Power Sources 239 (2013) 689–695.
[12] S. Sepasi, R. Ghorbani, B.Y. Liaw, Inline state of health estimation of lithium-ion batteries using state of charge calculation, J. Power Sources 299 (2015) 246–254.
[13] C. Hu, B.D. Youn, J. Chung, A multiscale framework with extended kalman filter for lithium-ion battery SOC and capacity estimation, Appl. Energy 92 (2012) 694–704.
[14] Y. Zou, X. Hu, H. Ma, S.E. Li, Combined state of charge and state of health estimation over lithium-ion battery cell cycle lifespan for electric vehicles, J. Power Sources 273 (2015) 793–803.
[15] G.L. Plett, Extended kalman filtering for battery management systems of lipb-based hev battery packs: Part 3. state parameter estim, J. Power sources 134 (2) (2004) 277–292.
[16] W. Waag, C. Fleischer, D.U. Sauer, Critical review of the methods for monitoring of lithium-ion batteries in electric and hybrid vehicles, J. Power Sources 258 (2014) 321–339.
[17] V. Klass, M. Behm, G. Lindbergh, A support vector machine-based state-of-health estimation method for lithium-ion batteries under electric vehicle operation, J. Power Sources 270 (2014) 262–272.
[18] C. Sbarufatti, M. Corbetta, M. Giglio, F. Cadini, Adaptive prognosis of lithium-ion batteries based on the combination of particle filters and radial basis function neural networks, J. Power Sources 344 (2017) 128–140.
[19] M. Berecibar, F. Devriendt, M. Dubarry, I. Villarreal, N. Omar, W. Verbeke, J. Van Mierlo, Online state of health estimation on nmc cells based on predictive analytics, J. Power Sources 320 (2016) 239–250.
[20] J. Wu, Y. Wang, X. Zhang, Z. Chen, A novel state of health estimation method of Li-ion battery using group method of data handling, J. Power Sources 327 (2016) 457–464.
[21] J.P. Christophersen, S.R. Shaw, Using radial basis functions to approximate battery differential capacity and differential voltage, J. Power Sources 195 (4) (2010) 1225–1234.
[22] M. Dubarry, C. Truchot, B.Y. Liaw, Synthesize battery degradation modes via a diagnostic and prognostic model, J. power sources 219 (2012) 204–216.
[23] I. Bloom, A.N. Jansen, D.P. Abraham, J. Knuth, S.A. Jones, V.S. Battaglia, G.L. Henriksen, Differential voltage analyses of high-power, lithium-ion cells: 1.

technique and application, Appl. J. Power Sources 139 (1) (2005) 295–303.
[24] M. Dubarry, B.Y. Liaw, Identify capacity fading mechanism in a commercial $LiFePO_4$ cell, J. Power Sources 194 (1) (2009) 541–549.
[25] I. Bloom, J. Christophersen, K. Gering, Differential voltage analyses of high-power lithium-ion cells: 2. applications, J. Power Sources 139 (1) (2005) 304–313.
[26] I. Bloom, J.P. Christophersen, D.P. Abraham, K.L. Gering, Differential voltage analyses of high-power lithium-ion cells: 3. another anode phenomenon, J. power sources 157 (1) (2006) 537–542.
[27] M. Dubarry, C. Truchot, M. Cugnet, B.Y. Liaw, K. Gering, S. Sazhin, D. Jamison, C. Michelbacher, Evaluation of commercial lithium-ion cells based on composite positive electrode for plug-in hybrid electric vehicle applications. part I: initial characterizations, J. power sources 196 (23) (2011) 10328–10335.
[28] M. Dubarry, B.Y. Liaw, M.-S. Chen, S.-S. Chyan, K.-C. Han, W.-T. Sie, S.-H. Wu, Identifying battery aging mechanisms in large format li ion cells, J. Power Sources 196 (7) (2011) 3420–3425.
[29] X. Han, M. Ouyang, L. Lu, J. Li, Cycle life of commercial lithium-ion batteries with lithium titanium oxide anodes in electric vehicles, Energies 7 (8) (2014) 4895–4909.
[30] I. Bloom, L.K. Walker, J.K. Basco, D.P. Abraham, J.P. Christophersen, C.D. Ho, Differential voltage analyses of high-power lithium-ion cells. 4. cells containing NMC, J. Power Sources 195 (3) (2010) 877–882.
[31] C. Weng, Y. Cui, J. Sun, H. Peng, On-board state of health monitoring of lithium-ion batteries using incremental capacity analysis with support vector regression, J. Power Sources 235 (2013) 36–44.
[32] T. Goh, M. Park, M. Seo, J.G. Kim, S.W. Kim, Capacity estimation algorithm with a second-order differential voltage curve for li-ion batteries with nmc cathodes, Energy 135 (2017) 257–268.
[33] IEC61434, Secondary Cells and Batteries Containing Alkaline or Other Non-acid Electrolytes - Guide to Designation of Current in Alkaline Secondary Cell and Battery Standards, International Standard 1996-10-03, (1996).
[34] X. Feng, J. Li, M. Ouyang, L. Lu, J. Li, X. He, Using probability density function to evaluate the state of health of lithium-ion batteries, J. Power Sources 232 (2013) 209–218.
[35] B. Potter, T. Duong, I. Bloom, Performance and cycle life test results of a peve first-generation prismatic nickel/metal-hydride battery pack, J. power sources 158 (1) (2006) 760–764.
[36] X. Li, J. Jiang, L.Y. Wang, D. Chen, Y. Zhang, C. Zhang, A capacity model based on charging process for state of health estimation of lithium ion batteries, Appl. Energy 177 (2016) 537–543.
[37] R.L. Hartmann II, An Aging Model for Lithium-ion Cells, Ph.D. thesis The University of Akron, 2008.
[38] D.E. Seborg, D.A. Mellichamp, T.F. Edgar, F.J. Doyle III, Process Dynamics and Control, John Wiley & Sons, 2010.
[39] S.W. Smith, The Scientist and Engineer's Guide to Digital Signal Processing, California Technical Pub, 1999.
[40] C. Weng, X. Feng, J. Sun, H. Peng, State-of-health monitoring of lithium-ion battery modules and packs via incremental capacity peak tracking, Appl. Energy 180 (2016) 360–368.
[41] J. Vetter, P. Novák, M. Wagner, C. Veit, K.-C. Möller, J. Besenhard, M. Winter, M. Wohlfahrt-Mehrens, C. Vogler, A. Hammouche, Ageing mechanisms in lithium-ion batteries, J. power sources 147 (1) (2005) 269–281.
[42] A. Barré, B. Deguilhem, S. Grolleau, M. Gérard, F. Suard, D. Riu, A review on lithium-ion battery ageing mechanisms and estimations for automotive applications, J. Power Sources 241 (2013) 680–689.
[43] Y. Kobayashi, T. Kobayashi, K. Shono, Y. Ohno, Y. Mita, H. Miyashiro, Decrease in capacity in mn-based/graphite commercial lithium-ion batteries i. imbalance proof of electrode operation capacities by cell disassembly, J. Electrochem. Soc. 160 (8) (2013) A1181–A1186.
[44] K. Jalkanen, J. Karppinen, L. Skogström, T. Laurila, M. Nisula, K. Vuorilehto, Cycle aging of commercial nmc/graphite pouch cells at different temperatures, Appl. Energy 154 (2015) 160–172.
[45] Y.W. Zeng, Investigation of $LiNi_{1/3}Co_{1/3}Mn_{1/3}O_2$ cathode particles after 300 discharge/charge cycling in a lithium-ion battery by analytical tem, J. Power Sources 183 (1) (2008) 316–324.
[46] B. Stiaszny, J.C. Ziegler, E.E. Krauß, M. Zhang, J.P. Schmidt, E. Ivers-Tiffée, Electrochemical characterization and post-mortem analysis of aged$LiMn_2O_4 - NMC/graphite$ lithium ion batteries part ii: calendar aging, J. Power Sources 258 (2014) 61–75.
[47] I. Buchberger, S. Seidlmayer, A. Pokharel, M. Piana, J. Hattendorff, P. Kudejova, R. Gilles, H.A. Gasteiger, Aging analysis of graphite/$LiNi_{1/3}Co_{1/3}Mn_{1/3}O_2$ cells using XRD, PGAA, and AC impedance, J. Electrochem. Soc. 162 (14) (2015) A2737–A2746.
[48] G. Sarre, P. Blanchard, M. Broussely, Aging of lithium-ion batteries, J. Power Sources 127 (1) (2004) 65–71.
[49] P. Niehoff, E. Kraemer, M. Winter, Parametrisation of the influence of different cycling conditions on the capacity fade and the internal resistance increase for lithium nickel manganese cobalt oxide/graphite cells, J. Electroanal. Chem. 707 (2013) 110–116.
[50] M. Dubarry, C. Truchot, B.Y. Liaw, K. Gering, S. Sazhin, D. Jamison, C. Michelbacher, Evaluation of commercial lithium-ion cells based on composite positive electrode for plug-in hybrid electric vehicle applications III. effect of thermal excursions without prolonged thermal aging, J. Electrochem. Soc. 160 (1) (2013) A191–A199.
[51] C. Truchot, M. Dubarry, B.Y. Liaw, State-of-charge estimation and uncertainty for lithium-ion battery strings, Appl. Energy 119 (2014) 218–227.
[52] M. Dubarry, C. Truchot, B.Y. Liaw, K. Gering, S. Sazhin, D. Jamison, C. Michelbacher, Evaluation of commercial lithium-ion cells based on composite positive electrode for plug-in hybrid electric vehicle applications. part ii. degradation mechanism under 2C cycle aging, J. Power Sources 196 (23) (2011) 10336–10343.
[53] M. Dubarry, A. Devie, B.Y. Liaw, The value of battery diagnostics and prognostics, J. Energy Power Sources 1 (5) (2014) 242–249.
[54] R. Jung, M. Metzger, F. Maglia, C. Stinner, H.A. Gasteiger, Oxygen release and its effect on the cycling stability of linixmnycozo2 (nmc) cathode materials for Li-ion batteries, J. Electrochem. Soc. 164 (7) (2017) A1361–A1377.
[55] W.-H. Ryu, S.-J. Lim, W.-K. Kim, H. Kwon, 3-D dumbbell-like $LiNi_{1/3}Co_{1/3}Mn_{1/3}O_2$ cathode materials assembled with nano-building blocks for lithium-ion batteries, J. Power Sources 257 (2014) 186–191.
[56] J. Xu, S.-L. Chou, Q.-f. Gu, H.-K. Liu, S.-X. Dou, The effect of different binders on electrochemical properties of $LiNi_{1/3}Co_{1/3}Mn_{1/3}O_2$ cathode material in lithium ion batteries, J. Power Sources 225 (2013) 172–178.
[57] X. Han, M. Ouyang, L. Lu, J. Li, Y. Zheng, Z. Li, A comparative study of commercial lithium ion battery cycle life in electrical vehicle: aging mechanism identification, J. Power Sources 251 (2014) 38–54.
[58] P. Keil, S.F. Schuster, J. Wilhelm, J. Travi, A. Hauser, R.C. Karl, A. Jossen, Calendar aging of lithium-ion batteries i. impact of the graphite anode on capacity fade, J. Electrochem. Soc. 163 (9) (2016) A1872–A1880.